

Control of the near-wake flow around a circular cylinder with electrohydrodynamic actuators

G. Artana, R. Sosa, E. Moreau, G. Touchard

580

Abstract We analysed the modifications of the near wake of a circular cylinder ($2,300 < Re < 58,000$) when the flow was perturbed steadily using an electrohydrodynamic actuator. Two electrodes flush-mounted on the surface of the cylinder were excited with DC power supplies to create a plasma sheet contouring the body. The discharge produced an electric force and changed the physical properties in the fluid layers at close vicinity to the surface. This plasma sheet diminished the base pressure, modified the size of the mean recirculation region and produced an increase in the shear stresses of the layers bounding the contour of this region.

1 Introduction

The separated boundary layer produced on the disturbed flow taking place around a circular cylinder continues to develop downstream as free shear layers. These free shear layers initially border a region with a static pressure lower than in the undisturbed stream, usually designated as the near-wake region (Zdravkovich 1997).

The near-wake flows develop a complex configuration of instabilities that are largely dependent on the Reynolds number Re considered. For the Re range analyzed in this article ($2,300 < Re < 58,000$), different authors (Bloor 1963; Chyu et al. 1995) have pointed out that the near-wake flows exhibits two coexisting modes: the shear layer mode and the Karman mode.

The shear layer mode is associated with the onset of a Kelvin–Helmholtz instability in the free shear layer formed from the surface of the cylinder. This instability eventually leads to small-scale vortices that may interact with large-scale ones.

The Karman or sinuous mode has been largely studied as it is responsible for the dynamic loading of the body produced by the large-scale vortex shedding. Reports of the last decade have especially described (Huerre and Monkewitz 1990) the way this mode can act as a “wave-maker” with frequencies produced by a self-excited oscillation. This oscillation is produced by the appearance of a global instability in the near wake originated by a pocket of an absolute unstable region.

The control of the development of wake flow instabilities can be achieved with the use of actuators. The excitation to be introduced in the flow may have a steady or a dynamic (with variable frequencies, amplitudes or signal forms) character. The selection of a steady or a dynamic excitation of the flow with small-amplitude perturbations depends on the instability characteristics.

The most common method to modify the wake dynamics consists of steady or quasi-steady modifications of the boundary conditions. Somewhat fewer efforts involving unsteady open-loop forcing or closed-loop (feedback) control devices have been proposed. This is probably because in practical applications they represent an increase in complexity vis-à-vis the steady methods.

Different actuators such as steady or unsteady blowing or suction, transverse cylinder oscillations, rotating cylinder oscillations and Lorentz force devices have been proposed to perform flow control around cylinders. A review of the different kinds of actuators was published previously (Meier 1996).

Electrohydrodynamic (EHD) actuators based on momentum transfer through electric forces have been studied at different laboratories. These devices involve small power consumption, and currents flowing in the system are so low that the magnetic effects may be disregarded. These actuators have also important advantages, namely simplicity, reliability (they have no moving parts) and a very short electrical response time (theoretically lower than 1 ns).

The use of EHD actuators in an electrically neutral fluid requires creation of ions in the fluid flow. This is generally performed by means of an electrical discharge. The ions under the action of coulombic forces drift towards the electrode of opposite sign and exchange momentum with the neutral fluid particles via particle collision. If the

Received: 9 May 2003 / Accepted: 27 July 2003
Published online: 25 October 2003
© Springer-Verlag 2003

G. Artana (✉), R. Sosa
Fluid Dynamics Laboratory,
Department of Mechanical Engineering,
Faculty of Engineering,
University of Buenos Aires,
CONICET, Buenos Aires,
Argentina
E-mail: gartana@fi.uba.ar
Fax: +54-11-43311852

E. Moreau, G. Touchard
Laboratoire d'Etudes Aérodynamiques (UMR 6609 CNRS),
University of Poitiers,
Futuroscope Cedex, France

This research was supported by the UBACYT AI-03 and PICT 2000–2001 12-482 grants from the Argentine government.

electrodes of the EHD actuator are flush-mounted on the surface of the body, most of the momentum transfer should take place in fluid layers that have a very low kinetic energy. In this way, with little power added to the flow, we can expect to observe important changes in the fluid dynamics.

Research concerning EHD actuators has mostly explored the possibility of modifying the flow around flat plates. Malik et al. (1983) and Bushnell (1983) proposed a device consisting of needles placed normally to a flat plate with their tips lying on the wall surface. When the device was operated, it produced an increase in the air momentum mainly in the direction of the normal to the surface. Considering the continuity equation, it can be demonstrated that this increase produces a reduction of the longitudinal momentum and a reduction of the velocity gradient at the wall. Some authors (Roth and Sherman 1998, 2000) indicated that this technique is probably limited to low Reynolds number applications due to limitations on scaling the corona discharge effect to the high flow velocities of flight conditions.

More efficient devices that add momentum tangentially to the wall have recently been developed. With these kinds of systems, a more uniform action and major control of the ion trajectories can be achieved. Roth and Sherman (1998, 2000) proposed a device named “one atmosphere uniform glow discharge” (OAUGDP). The system uses electrodes separated by an insulating surface that avoids knocking the ions on the cathode. In this way, cathode heating and the formation of new avalanches or breakdown from electron secondary emission, which can lead to nonuniform discharges, is prevented. Similar devices (Scherbakov et al. 2000) and others using a pulsed excitation have been recently studied (Corke and Mattalis 2000; Corke et al. 2002; Lorber et al. 2000; Johnson and Scott 2001; Hultgren and Ashpis 2003; Wilkinson 2003).

On the other hand, devices with bare electrodes without any dielectric barrier have also been proposed (Soetomo 1992; El-Khabiry and Colver 1997; Colver and El-Khabiry 1999). They consist of two electrodes flush-mounted on the same side of an insulating surface of a flat plate, enabling the creation of a bipolar corona discharge with a DC voltage excitation.

The experimental studies were complemented with numerical simulations of the flow considering a very small diameter (2 μm) wire-wire electrode configuration. The numerical simulations predicted a corona thinning for the boundary layer and a reduction in the drag of the flat plate, although the latter was almost one order of magnitude larger than the experimentally verified results.

Other devices without dielectric barriers but with very well finished wire-wire (Léger et al. 2002a, 2002b) or wire-plate electrodes (Desimone et al. 1999; Desimone 2000; Artana et al. 1999, 2000, 2001, 2002; Léger et al. 2000, 2001) are now being considered. Under suitable operation, these devices minimize the problems of spot formation, and uniform discharges can be achieved. Moreover, depending on the excitation, it is possible to obtain a discharge regime characterized by a uniform plasma sheet contouring the body surface that occupies the whole interelectrode space (generalized glow regime).

The mechanism of interaction discharge-airflow associated with momentum transfer by ion collision is inherent to this actuator, but others may also be involved.

Depending on intensity, the ionization of a gas may produce important alterations of the mechanical properties of the fluid (like density, viscosity and so on). As the plasma sheet devices produce uniform ionization of fluid layers at close vicinity to the walls, the resulting alteration of fluid properties in this region may effectively constitute an effective electromechanical coupling mechanism.

A refined electrical model that could clarify the different mechanisms governing the establishment and characteristics of this discharge regime, and so of its interaction with the airflow, is still missing. Considering the theory of streamer's phenomena, it may be argued that a uniform plasma sheet, although it is produced by a DC excitation, could be a pulsating discharge with a repetition of some kilohertz. Research is now being developed by our group to elucidate this question.

The goal of this work is to determine the flow modifications of an airflow around a circular cylinder under a steady excitation of the fluid at close vicinity to the surface with an EHD actuator operating in the generalized glow regime. We analyze a wide range of the flow regimes characterized by transition to turbulence of the shear layers ($2300 < Re < 58000$).

2 Evaluation of flow modifications

The development of devices to control the wake flow requires quantification of the qualitative observations deduced from visualizations. In this aspect, the study of time-averaged magnitude is a powerful tool to compare the capabilities of the different actuators as they bring out essential information. In the case of wake flows, it is of particular interest to time-average the magnitudes of velocity or pressure over large periods of time compared to the shedding period.

The time-averaging of the velocity field in the near wake enables us to determine a “mean recirculation region” that characterizes the vortex shedding regimes. This region is symmetric and closed, and it is possible to define within it a bubble length L_b and a bubble width d_b .

The length of such region has usually been obtained by the experimental measurement of the eddy formation length L_f defined by the distance downstream from the cylinder axis to the point where the rms velocity fluctuations are maximized on the wake central line.

In the last decade, the development of the particle-image velocimetry (PIV) technique has allowed for easier determination of the magnitudes of L_b and d_b . For this determination, the use of the PIV technique requires a suitable choice of the duration and sampling of the experiment.

Furthermore, time-averaging of the surface pressure on the base of the cylinder has received special attention. Different authors (Roshko 1993; Norberg 1994; Williamson 1996) considered this magnitude as a convenient and meaningful reference for discussion of the phenomena of bluff body aerodynamics. This is mainly because there is a close connection between this coefficient and the drag, but

also because it highlights different aspects of the wake dynamics in a very large range of Re values.

The averaged flow field and surface pressure are not independent parameters (Unal and Rockwell 1988). The magnitude of the base pressure is usually expected to be related to the strength of the vortex formed from the body and also to the length required to complete their formation. The relationship between these parameters was partially clarified when Roshko established with a simplified model a link between the bubble length of the mean recirculation region and the base pressure (Roshko 1993; Norberg 1994; Williamson 1996). In order to characterize the behavior of the near-wake region our study is based on the time-averaged values of the flow field and of the surface pressure.

3 Experimental setup

3.1 Wind tunnel and cylinders

The flow visualization experiments were undertaken at low flow velocities with the cylinder placed in a small open wind tunnel (0–5-m/s, $0.28 \times 0.28\text{-m}^2$ rectangular cross section). For surface pressure distributions and flow field velocimetry, the measurements were done in a wind tunnel loop that enabled testing at higher flow velocities (1–30 m/s, $0.50 \times 0.50\text{-m}^2$ rectangular cross section). The cylinder was placed in the test section with the axis horizontal and normal to the main flow with a turbulence intensity lower than 0.5% (5000 Hz). The characteristics of these tunnels have been published previously (Tensi et al. 2002)

In our study the electrodes were flush-mounted on the surface of polymethyl methacrylate cylinders that were 32 mm in diameter D (length $L = 500$ mm, $L/D = 15.6$; and $L = 280$ mm, $L/D = 11.4$). The cylinder was a hollow tube with a 3-mm thick wall. Two electrodes were used: a wire one (0.90-mm diameter) and a planar one, which was a thin aluminum foil (50- μm thick). Both electrodes were parallel to the cylinder axis (Fig. 1). The ends of both electrodes were rounded to avoid a large field concentration.

The cylinder was oriented such that the wire electrode occupied the frontal stagnation point ($\theta = 0^\circ$). The cylinder was fixed on both ends through pieces of electrical insulating material (nylon) entering in the hollows of the tube. The blockage ratio was 11.4% in the open wind tunnel and 6.4% in the wind tunnel loop. No correction for blockage effects has been applied to the data.

3.2 EHD excitation

Two independent adjustable high-voltage sources of opposite polarities (+40 kV, –40 kV, 3.75 mA) were used to apply a voltage difference high enough to sustain a stable discharge. The wire electrode was connected to the positive polarity source, and the plate electrode to the negative one. By increasing the voltage difference between both electrodes, different discharge regimes could then be established. The current measurement was undertaken with an electrometric circuit that could detect currents of 1 nA.

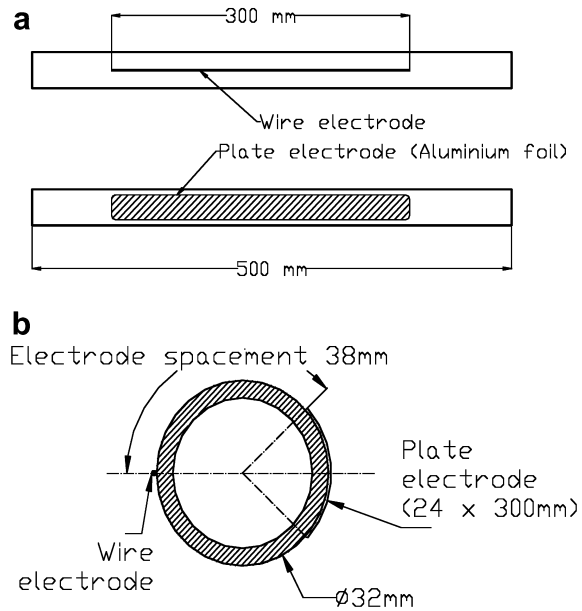


Fig. 1. a Schematic of the electrode configuration. b Schematic of the electrode configuration (side view)

3.3 Flow visualizations

For flow visualizations, a smoke injection technique was used. The device comprised a laser sheet produced by a 5-W argon-ion laser and a single smoke filament ($\phi_f = 2$ mm). The seeding was produced with a smoke generator (EI 514 Deltalab) that used pure cosmetic-grade oil. The images of the streaklines of the flow were recorded with a video camera at 30 frames per second and then digitalized.

3.4 Velocity field measurements

The velocity field was measured using a particle-image velocimetry (PIV) technique. These experiments were conducted using the DANTEC system controlled by FlowMap PIV. The system was adjusted to obtain interrogation areas of 32×32 pixels with an overlap of 50%. The smoke generator used in these sets of experiments was the same previously described in Sect. 3.3.

The system was illuminated with a laser sheet produced by a 200-mJ YAG laser. In our experiments each pulse had a 0.01- μs duration and the time between a pair of pulses was 50 μs . A progressive scan interline camera capable of producing images of 768×484 pixels was used. Six hundred pairs of digital images taken every 0.1 s were examined in each experiment. The images were obtained with a scale factor of 10.4.

The system resolution for distances can be estimated as the product of the pixel resolution (1/4 pix) and the pixel size. In that way, the resolution of the velocity field can be estimated dividing the latter value by the time between a pair of pulses. In our case the pixel size was about 0.125 mm, leading to a conservative value of uncertainty for the velocity of $\Delta v = \frac{1}{4} \text{pix} \cdot \frac{1 \text{ mm}}{8 \cdot \text{pix}} \cdot \frac{1}{50 \mu\text{s}} \cong 0.6 \text{ m/s}$.

Each velocity field was filtered with both a peak-validation and a range-validation filter. The peak validation

filter is based on the detectability criterion (Keane and Adrian 1992). It validates vectors with a ratio of the highest peak to the second-highest peak in the correlation plane larger than a fixed value (1.2 in our case). The range-validation filter enables us to establish the range admitted for the modulus of the velocity vectors. In our case, we considered a maximum value of 2.5 times the flow velocity U_0 as the upper limit. Undertaking these filtering processes, about 5% to 10% of the vectors were removed from the 1363 initial vectors.

3.5 Particle tracking

The trajectories of the seeding particles and those of the fluid particles surrounding the tracer have frequently been considered to be the same in flow visualizations by smoke injection techniques and in PIV experiments. However, if a slipping velocity is verified between the tracer and the fluid, the trajectories might differ. The tracer particles could “swim” in the moving media, and the information obtained from the tracers must then be carefully examined.

In our experiments, the seeding was produced with the smoke generator operated to obtain a cloud with a mean particle diameter of 0.3 μm . As analyzed in a previous article (Artana et al. 2002), the influence of coulombic forces on the tracer trajectory when using seeding particles of this size can be disregarded without introducing a significant error.

3.6 Pressure measurements

For the surface pressure distribution experiments, we used a similar cylinder but with 20 small orifices on its surface (Fig. 2). The pressure tapping hole diameters considered were 1 mm, and their centers were equally spaced at 9° . Electrical insulating Tygon tubes passing through the inside of the cylinder hollow enabled us to connect the orifices with the pressure sensors.

A set of 20 independent solid state sensors (ion-implanted piezoresistive strain gage) with their outputs connected to a data acquisition system were used. At low velocities (<5 m/s) the typical integration time was about 10 s. However, at higher velocities this time could be significantly reduced.

The free stream velocity U_0 was measured with a pitot-static tube positioned 0.5-m upstream of the cylinder connected to a micromanometer. The pressure can be rendered dimensionless with the dynamic pressure. We consider a coefficient C_p defined as

$$C_p = \frac{P - P_0}{\rho U_0^2 / 2}, \tag{1}$$

where P is the pressure on the surface of the cylinder, P_0 is the static pressure of the free airstream, and ρ is the gas density.

The coefficient obtained at the position corresponding to an angle $\theta = 180^\circ$ was taken as the base pressure coefficient C_{pb} , and the negative of this quantity ($-C_{pb}$) is referred to as the base suction coefficient.

3.7 Time-averaging of magnitudes

In our case, the mean velocity field of the airflow is obtained by averaging the instantaneous flow fields over 60 s. In the flow regime considered, the Strouhal number St is close to 0.2 and is calculated as:

$$St = \frac{f_s D}{U_0}. \tag{2}$$

As a result, when comparing the shedding frequency f_s with the duration of our experiment and the sampling frequency considered, it can be assured that the time-averaged values obtained converge to the mean value.

4 Results and discussion

4.1 Discharge characteristics

A typical voltage–current curve from our experiments is shown in Fig. 3 (results are shown considering current per unit length of the electrodes). In this figure distinct zones could be distinguished based upon the different behaviors or regimes exhibited by the discharge. The different regimes observed were similar to those described in our previous works (Artana et al. 1999; Desimone et al. 1999).

The first type of regime corresponded to the first part of the curve under very low currents (lower than 0.2 $\mu\text{A}/\text{m}$), in which the corona discharge was almost negligible. This regime occurred for voltage differences lower than values of approximately 25 kV.

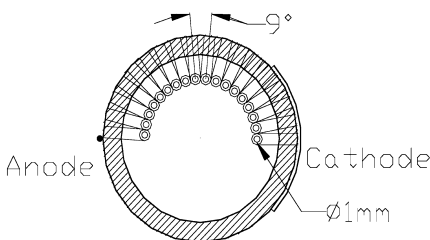


Fig. 2. Side view of the disposition of pressure tubes

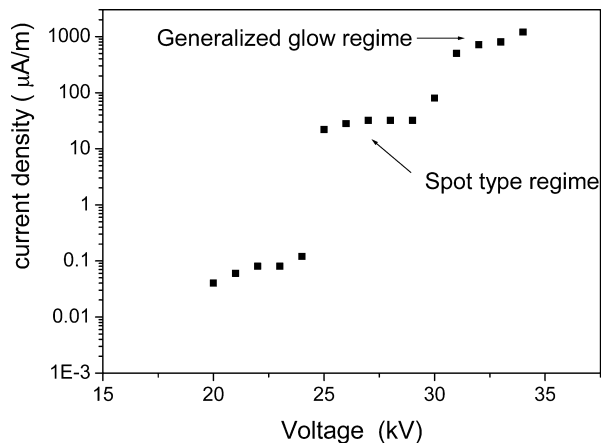


Fig. 3. Voltage versus current per unit electrode length

At higher voltage differences, we could observe two different zones with distinctive discharge regimes having the following characteristics:

- *Spot-type regime*: The discharge was concentrated on some visible spots on the wire. The spot number increased with the applied voltage difference. Some of them might ionize in a plume-like type or might lead to a narrow channel attached to the surface. In Fig. 3 this regime corresponded to currents lower than 0.1 mA/m and to voltages lower than about 30 kV.
- *Generalized glow regime*: The picture of this regime shown in Fig. 4 was obtained by darkening the room. The regime was characterized by a homogeneous luminescence covering the cylinder surface. The luminescence occupied the whole interelectrode region and made the cylinder look like it supported a thin film of ionized air. By visual inspection it seemed that the thickness of the ionized sheet was of the order of the thickness of the aluminum foil (50 μm). In Fig. 3 this regime corresponded to voltages of about 30–35 kV and to currents between 0.4 and 2.5 mA/m. The discharge was homogeneous, showed little noise, and the current remained stable over long periods of time.

This regime could be obtained with adequate finishing of the electrode. Under other conditions, this regime might be absent and the spot-type regime could be followed by a filamentary-type regime or directly by a spark. For velocities up to 30 m/s the velocity of the airflow did not significantly modify the intensity of the current. At larger velocities, the generalized glow regime persisted in a wider range of voltages and higher currents could be attained.

In the present work, measurements with the actuator were undertaken operating exclusively in the generalized glow regime. A typical value of power consumption per unit area associated with this regime of about 500 W/m² could be recorded in our experiments. This value agreed with the power consumption needed to sustain a glow discharge with the OGADUP device as well as with the power consumption obtained with similar EHD actuators in a planar configuration.

4.2 Flow visualization

Zdravkovich (1997) proposed the classification of the different flow regimes around a circular cylinder as a

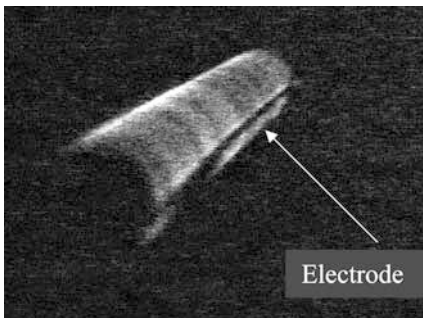


Fig. 4. Digitalized image of the generalized glow discharge. Plasma sheet contouring the cylinder surface, $\Delta V=34$ kV

function of Reynolds number. According to this classification, our flow visualization experiments were undertaken in the intermediate subcritical regime of transition in the shear layer state ($1-2k < Re < 20-40k$). The near wake in this flow state is surrounded by initially laminar free shear layers. However, as Re increases this regime shows undulations in the shear layer (transition waves) that roll up into discrete eddies (transition eddies) along the free shear layer before becoming turbulent. The transition region may move with increasing Re along the free shear layer towards the separation region and affects the length and the width of the near wake.

Figure 5 shows photos of typical visualizations for the low-velocity range ($Re \approx 2500$), with discharge off (Fig. 5a, at $t = -0.04$ s) and discharge on (Fig. 5b, at 1.6 s after the electric field is applied at time $t = 0$). The wire electrode was placed on the frontal stagnation point (at left in the photo) and the plate electrode was opposed at 180°.

After a short period of time, the nonperturbed flow region disappeared and was convected by the flow, establishing a new flow condition in the near wake (Fig. 5b). In this way, the transition region in the separated shear layer seemed closer to the cylinder. The eddy formation region was largely perturbed and the vortex streets could no longer be easily detected.

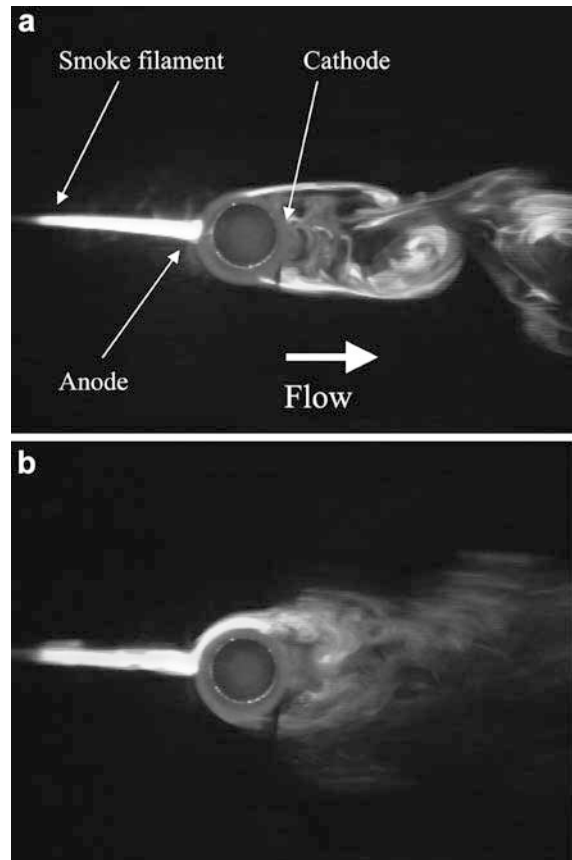


Fig. 5a, b. Sequence of visualizations: a $t = -0.04$ s, $U_0 = 0.7$ m/s. b $t = 1.56$ s (electric field is applied at $t = 0$), $U_0 = 0.7$ m/s, $\Delta V = 32$ kV

4.3

Time-averaged velocity fields

For experiments using the PIV technique, larger flow velocities than those used in flow visualization were employed. According to Zdravkovich's classification, these experiments were conducted in the upper subcritical regime of the transition in the shear layer state ($20-40k < Re < 100-200k$). The regime is characterized by an almost immediate transition to turbulence of the separated shear layer that is accompanied by a very short near wake, which is almost constant in size in the whole Re range of this regime.

Figure 6 (actuator off and on, respectively, in Figs. 6a and 6b), shows typical results of the mean velocity field for the displaced and near-wake regions. These results were obtained at $U_0=16.7$ m/s ($Re \approx 35,500$), and similar results were obtained at different velocities in the range considered for the PIV experiments (10–20 m/s). Figure 6 shows that two counter-rotating vortexes were observed in the time-averaged field. The contour enclosing these cells enables us to define the limits of the mean recirculation region. A careful look at these figures, in contrast to what occurred at the low-velocity range of the flow visualization experiments, shows that the actuator causes only a very slight narrowing and a shortening of the bubble enclosed in this region.

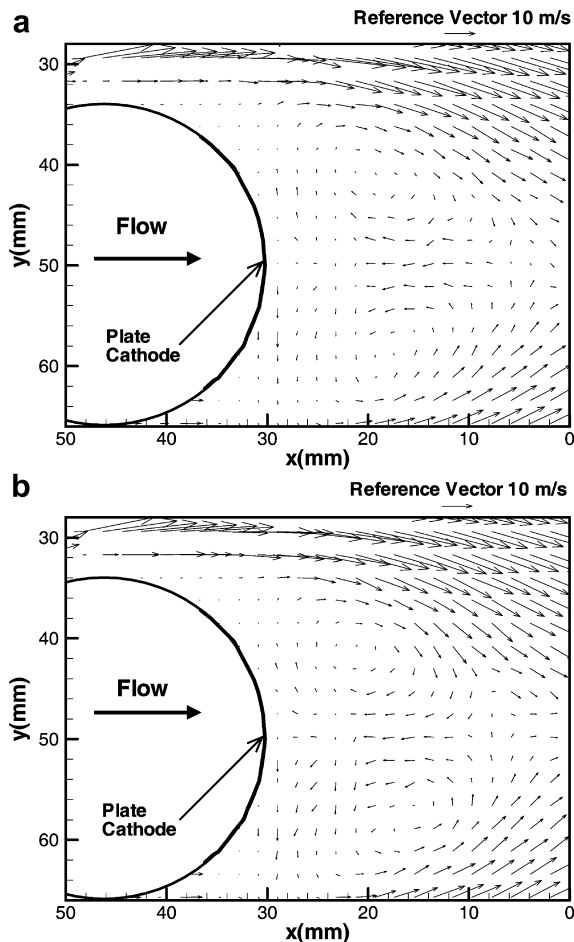


Fig. 6a, b. Time-averaged velocity field in the near wake: a Voltage off, $U_0=16.7$ m/s. b Voltage on, $U_0=16.7$ m/s, $\Delta V=34$ kV

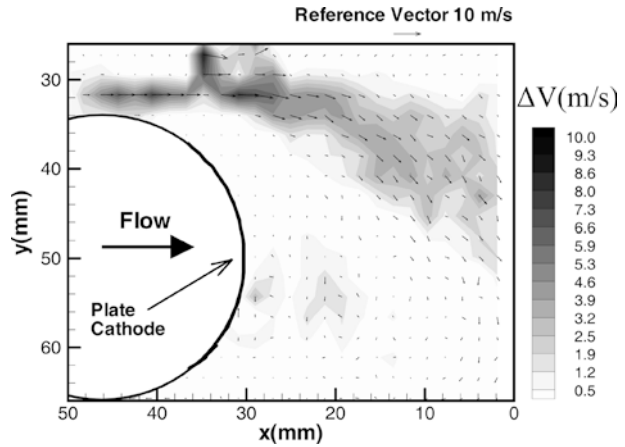


Fig. 7. Time-averaged velocity field difference in the near-wake region (voltage on–voltage off), $U_0=16.7$ m/s, $\Delta V=34$ kV

To highlight the effect of the actuator on the flow, contour and vector diagrams of the difference between the time-averaged velocities with the electric field on and off were plotted in Fig. 7. Figure 7 reveals an important acceleration in the zone close to the separated shear layer and also in fluid layers close to the cylinder surface. In the range tested, the maximum difference attained values of about 8.5 m/s (almost a half of the incident flow velocity).

In our previous reports (Artana et al. 2000, 2001, 2002; Léger et al. 2000) the changes in the velocity profiles in a cylindrical and flat plate flow configuration were characterized. Our results indicated that the changes in the momentum close to the wall were governed simultaneously by diffusion (mainly in the direction of the normal to the surface) and by convection processes (mainly in the flow direction). Prior to separation, the diffusion was not very important, and the streamlines that were far from the surface “suffered” the effect of the boundary changes less than those taking place closer to it. Under a boundary layer separation, the convection enabled these effects to penetrate more deeply in the flow field, comprising the zones enclosing the mean recirculation region.

4.4

Surface pressure distribution

Figure 8 shows the results of the changes in the cylinder surface pressure in the presence of the discharge for different electrical currents. The results correspond to $Re \approx 21,600$ (Fig. 8a) and $Re \approx 57,600$ (Fig. 8b). These figures reveal a similar surface pressure distribution of the flows independent of the actuator being on or off. Note that the curves have minima, and beyond these minima there is a pressure rise followed by a plateau that is usually associated with the boundary layer separation. As seen in Fig. 8 the actuator produced no significant changes either on the position of the measurement point where the minimum occurs, or in the position where the plateau appeared. In consequence, from our experiments it was not possible to ascribe a role to the discharge in the production of changes in the position of the separation line of the boundary layer.

Even though the curves are similar, the presence of the actuator could induce differences in the value of the

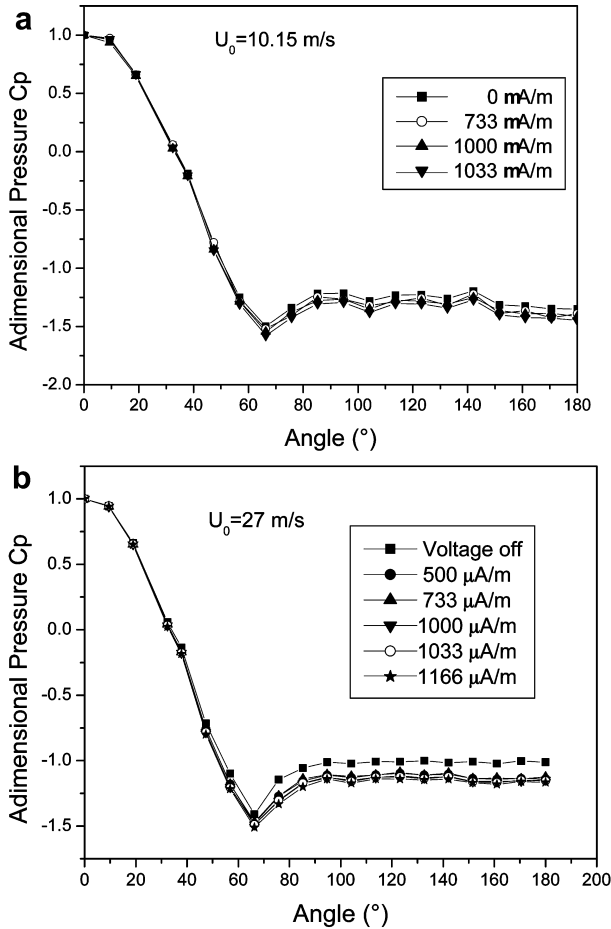


Fig. 8a, b. Pressure distribution on the cylinder surface: a $U_0=10.15$ m/s. b $U_0=27.0$ m/s

pressure for each measurement point. Effectively when the generalized glow regime was established, Fig. 8 shows that no significant changes could be detected in the regions where C_p was positive, but reductions in pressure (or increase in suction) were observed in almost all measurement points where C_p adopted negative values.

In the region where changes were observed, the incidence of the actuator's power depended on the flow regime. In the example of Fig. 8a (corresponding to airflow velocity of 10.15 m/s), the absolute value of the nondimensional pressure in the plateau changed gradually when power increased.

Conversely, based on the curves of Fig. 8b (corresponding to higher airflow velocities of 27.0 m/s), a jump in the values of the plateau verified that the generalized glow regime was established. However, by increasing the actuator power in this discharge regime no significant changes were produced in C_p , and the resulting curves for different powers were almost superposed. As an example, considering the values at $\theta = 180^\circ$, the $-C_{pb}$ for powers of 521.1 W/m² (1166 μ A/m) were only about 3% lower than the ones corresponding to 210.1 W/m² (500 μ A/m).

Consequently, these experiments indicated that the effect on surface pressure produced by the actuator operating in the generalized glow regime exhibited a dependency on the airflow velocity. The effect became

larger when the fluid flowed at high velocities, but simultaneously a saturation with power appeared at these regimes.

4.5

Base pressure coefficient

Based on the work of Sychev (1982), Roshko (1993) established a simplified model that links the bubble length of the mean recirculation region and the base pressure. Considering that the fluid inside the wake was in equilibrium between the pressure forces, and the shear stress τ acting on the boundary between the base of the body and the recirculation bubble (enclosed by the streamline $\varphi = 0$ of Fig. 9) he proposed

$$\int_{\varphi=0} p dy + \int_{\varphi=0} \tau dx = 0. \quad (3)$$

The model was originally developed for steady wake flows with no vortex shedding (such as in the case of cylinder with splitter plates), and it was then been extended to time-averaged flows with vortex shedding. In the analysis of these integrals, Roshko considered that the pressure at $\varphi = 0$ is almost constant with a value $p = p_b$ except near the reattachment point, where the pressure has the same value as that far from the cylinder ($p = p_0$). Also considering that the shear on the boundary has a constant value, it is then proposed

$$|p_b - p_0| d_b = 2 \tau L_b. \quad (4)$$

Though some authors (Williamson 1996) argued that this model needs an arbitrary choice of some parameters, its usefulness is recognized in clarifying the link between the base suction, the shear stresses and the recirculation length.

It was observed that the pressure difference appearing in Eq. (4) always adopts a negative value. In consequence, this model indicates that if the bubble width d_b is kept constant, a more negative value of the base pressure (or an increase of the base suction coefficient) leads to an increase in the second term of Eq. (4).

Figure 10 represents the base suction coefficient as a function of the Reynolds number with and without the discharge. Both curves have the same shape, and it is evident that the effect of the EHD actuator is to increase the value of the coefficient in the whole Re range tested.

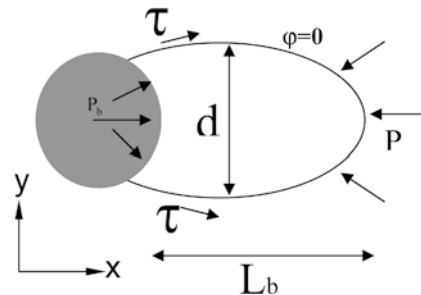


Fig. 9. Recirculation bubble defined by zero streamline of mean flow

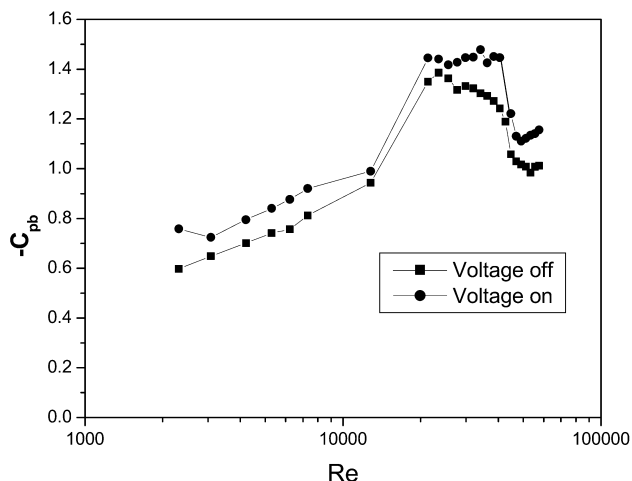


Fig. 10. Base suction coefficient versus Reynolds number, EHD actuator off (squares) and on (circles), $\Delta V=34$ kV

In the lower Re range, where flow visualization experiments were conducted, we observed an increase in the base suction accompanied by a shortening of the bubble length L_b . Undertaking an analysis with Roshko's model, this should be associated with a strong increase in the shear stresses. The strong acceleration of the flow produced by the discharge in the shear layer region is a manifestation of such augmentation.

Considering the larger Re numbers in which the PIV experiments were undertaken, our experiments indicated the existence of an increase in the base suction coefficient accompanied by almost no change in d_b and L_b . Considering Roshko's model when keeping the size of the mean recirculation region constant, an increase in the base suction is linked to an increase in the shear stresses on the boundary of this region. In our case, the acceleration of the separated shear layer as observed in Fig. 7 reflects the changes in the shear stresses predicted by the model. In conclusion, Roshko's simplified model for both the low- and high- Re range considered indicated that the EHD actuator produced an increase of the shear stresses of the layers bounding the near wake.

It seems reasonable, especially for high Reynolds numbers, that the increase in the shear stresses in the contour occurs as a consequence of a large increase in the Reynolds stresses ($\rho u'v'$). Unfortunately, the measurements of parameters characterizing turbulence could not be easily undertaken and we could not verify this hypothesis. In our configuration, the PIV technique was not a good tool to determine this parameters because of its low sampling rate and because the small-scale turbulent structures are much smaller than the size of the interrogation area. On the other hand, the existence of a discharge excluded the possibility of hot wire measurements mainly because of two reasons: ion attraction by the probe and the large amount of electromagnetic noise produced by the discharge.

5 Conclusions

We undertook our experiments in flow regimes around a cylinder identified by transitions of the shear layer (intermediate subcritical and upper subcritical regime).

Flow visualization experiments indicated that at relatively low Re -value regimes (intermediate subcritical regime), the effect of the discharge on the near-wake flow field is very important. The eddy formation region was largely perturbed, and vortex shedding phenomena could no longer clearly be observed.

The PIV measurements revealed that a strong acceleration in the regions of the separated shear layers might be induced. In the range of higher Re values (upper subcritical regime) such acceleration was also accompanied by a very small shortening and narrowing of the mean recirculation region. Even though the curves of pressure distribution displayed significant changes, from these results the capability of the actuator to affect the position of separation of the boundary layer could not be determined.

The pressure measurements however, indicated that the EHD actuator could substantially increase the base suction coefficient in the whole range of the Reynolds numbers tested. At high Re values a saturation of the effect with power was observed, indicating that from an energetic point of view there exists an optimum in the operation conditions of the actuator.

In our study the simple model developed by Roshko was revealed as a qualified tool to analyze the time-averaged flow parameters of the near wake, as it provided a straight link between the base pressure, the mean recirculation region size and the shear force acting on its contour. This model established that in our experiments the EHD actuator produced an increase in the shear stresses of the layers bounding the contour of this region. This increase in the shear probably occurred as a consequence of a significant increase in the Reynolds stresses, but so far no measurements support this hypothesis.

The present work established that the EHD actuator proposed was able to modify the flow in a large range of velocities. Additional experiments involving time-dependent behavior and focused on the boundary layer should be undertaken to better delimit strategies for steady and dynamic flow control with the use of the EHD devices.

References

- Artana G, Desimone G, Touchard G (1999) Study of the changes in the flow around a cylinder caused by electroconvection. In: *Electrostatics'99*, Philadelphia, pp 147-152
- Artana G, D'Adamo J, Desimone G, DiPrimio G (2000) Air flow control with electrohydrodynamic actuators. In: *Proc 2nd int workshop on conduction convection and breakdown in fluids*, Grenoble, pp 190-194
- Artana G, DiPrimio G, Moreau E, Touchard G (2001) Electrohydrodynamic actuators on a subsonic air flow around a circular cylinder. *AIAA paper 2001-3056*
- Artana G, D'Adamo J, Leger L, Moreau E, Touchard G (2002) Flow control with electrohydrodynamic actuators. *AIAA J* 9:1773-1779
- Bloor MS (1963) The transition to turbulence in the wake of a circular cylinder. *J Fluid Mech* 19:290-304
- Bushnell D (1983) Turbulent drag reduction for external flows. *AIAA paper* 83-0227
- Chyu C, Lin C, Sheridan J, Rockwell D (1995) Karman vortex formation from a cylinder: role of phase-locked Kelvin-Helmholtz vortices. *Phys Fluids* 7:2288-2290
- Colver G, El-Khabry S (1999) Modeling of DC corona discharge along an electrically conductive flat plate with gas flow. *IEEE Trans Ind Appl* 35:387-394

- Corke T, Mattalis E (2000) Phased plasma arrays for unsteady flow control. AIAA paper 2000-2323
- Corke T, Jumper E, Post M, Orlov D, McLaughlin T (2002) Applications weakly ionized plasmas as wing flow control devices. AIAA paper 2002-0350
- Desimone G (2000) Estudio experimental de la modificación del escurrimiento alrededor de un cilindro circular a través de la electroconvección. Dissertation, Facultad de Ingeniería, Universidad de Buenos Aires, Argentina
- Desimone G, DiPrimio G, Artana G (1999) Modification of the flow around a cylinder by means of electrodes placed on its surface. In: Proc colloque de la société Française d'électrostatique, Poitiers, pp 80-84
- El-Khabiry S, Colver G (1997) Drag reduction by D.C. corona discharge along an electrically conductive flat plate for small Reynolds number flows. *Phys Fluids* 9:587-599
- Huerre P, Monkewitz P (1990) Local and global instabilities in spatially developing flows. *Annu Rev Fluid Mech* 22:473-537
- Hultgren LS, Ashpis DE (2003) Demonstration of separation delay with glow-discharge plasma actuators. AIAA paper 2003-1025
- Johnson J, Scott S (2001) Plasma-aerodynamic boundary layer interaction studies. AIAA paper 2001-30523
- Keane R, Adrian R (1992) Theory of cross correlation analysis of PIV images. *Appl Sci Res* 49:191-215
- Léger L, Moreau E, Touchard G (2002a) Effect of a DC corona electrical discharge on the airflow along a flat plate. *IEEE Trans Ind Appl* 38:1478-1485
- Léger L, Moreau E, Touchard G (2002b) Electrohydrodynamic airflow control along a flat plate by a DC surface corona discharge—velocity profile and wall pressure measurements. AIAA paper 2002-2833
- Léger L, Moreau E, Artana G, Touchard G (2000) Modification de l'écoulement d'air autour d'une plaque plane par une décharge couronne. Colloque de la Société Française d'Electrostatique, Montpellier, pp 97-101
- Léger L, Moreau E, Artana G, Touchard G (2001) Influence of a DC corona discharge on the airflow along an inclined flat plate. *J Electrostat* 50/51:300-306
- Lorber P, McCormick D, Pollack M, Breuer K, Corke T, Anderson I (2000) Rotorcraft retreating blade stall control. AIAA paper 2000-2475
- Malik M, Weinstein L, Hussaini M (1983) Ion wind drag reduction. AIAA paper 83-0231
- Meier GEA (1996) Active control of boundary layer and separation. In: Meier GEA, Schnerr GH (eds) *Control of flow instabilities and unsteady flows*. Springer-Wien, New York, pp 203-233
- Norberg C (1994) An experimental investigation of the flow around a circular cylinder: influence of aspect ratio. *J Fluid Mech* 258:287-316
- Roshko A (1993) Perspectives on bluff body aerodynamics. *J Wind Ind Aerodyn* 49:78-79
- Roth JR, Sherman D (1998) Boundary layer flow control with a one atmosphere uniform glow discharge surface plasma. AIAA paper 98-0328
- Roth JR, Sherman D (2000) Electrohydrodynamic flow control with a glow discharge surface plasma. *AIAA J* 38:1166-1178
- Scherbakov Y, et al (2000) Drag reduction by AC streamer corona discharges along a wing-like profile plate. AIAA paper 2000-2670
- Soetomo F (1992) The influence of high voltage discharge on flat plate drag at low Reynolds number air flow. Dissertation, Iowa State University, Ames, IA, USA
- Sychev V (1982) Asymptotic theory of separated flows. *Mekh Zhidkosti i Gaza* 2:20-30
- Tensi J, Boué I, Paillé F, Dury G (2002) Modification of the wake behind a circular cylinder by using synthetic jets. *J Visualiz* 5:37-44
- Unal MF, Rockwell D (1988) On vortex formation from a cylinder. 1. The initial instability. *J Fluid Mech* 190:491-512
- Wilkinson SP (2003) Investigation of an oscillating surface plasma for turbulent drag reduction. AIAA paper 2003-1023
- Williamson CHK (1996) Vortex dynamics in the cylinder wake. *Annu Rev Fluid Mech* 28:477-539
- Zdravkovich M (1997) In: *Flow around circular cylinders*, vol 1. Oxford Science, Oxford, pp 1-18